

## ESTIMATION OF EARTHQUAKE MOTION INCIDENT ANGLE AT ROCK SITE

Takahiro SIGAKI<sup>1</sup>, Kazuhiko KIYOHARA<sup>2</sup>, Yoichi SONO<sup>3</sup>, Dai KINOSITA<sup>4</sup>, Toru MASAO<sup>5</sup>, Ryoichi TAMURA<sup>6</sup>, Chiaki YOSHIMURA<sup>7</sup> And Takeshi UGATA<sup>8</sup>

### SUMMARY

We proposed the calculation method for wave incident angle of actual earthquake motion. The developed method indicated obliquely incident waves near ground surface of rock site. On the other hand, the effect of the wave incident angle on structural responses is examined. As the result, it can be suggested that obliquely incident waves do not necessarily cause bad effects to the structure.

### INTRODUCTION

Seismic wave is refracted and reflected in the underground stratum many times before it reaches the ground surface. In general, as the surface soil is softer than the rock in the depths, seismic wave propagates vertically near the surface. However, it is considered that the incident wave at hard rock site, such as nuclear power station site, has the fluctuating angle when it reaches the base of structure. It is important for the seismic design of structures to investigate the incident angle of the input wave, because oblique input wave may cause severe vertical motions for the structure.

Strong-motion records have been collected at Sendai nuclear power station from start of commercial operation. The aim of this paper is to develop estimation method of wave incident angle from observed records in soil and to estimate it practically. Furthermore, the effect of wave incident angle on structural responses is investigated in order to obtain seismic design implications related to wave incident angle.

### OUTLINE OF STRONG-MOTION RECORDS USED FOR INVESTIGATIONS

Sendai site is located about 1,000 km west-southwest of Tokyo, Japan as mapped in Figure 1. Sendai nuclear power station (NPS) unit 1 is instrumented with 58 channel arrays by 27 sensors at outer shield (O/S), inner concrete (I/C), containment vessel (C/V), auxiliary building (A/B), fuel handling building (FH/B), ground surface and in rock as shown in Figure 2. Then, they provide horizontal (x and y direction) and vertical acceleration time history.

For our investigations, we used 24 strong-motion records of a peak horizontal acceleration at the top of reactor building (R/B) base mat over  $0.02 \text{ m/s}^2$  during the 1997 Kagoshima-ken hokuseibu earthquakes. These earthquakes occurred at about 20 km north-east of Sendai NPS site and included two mainshock-aftershock sequences. Although these earthquakes occurred successively on March 26 and May 13, 1997, in same area, it is considered that these are different earthquakes because of different focal mechanism. Location and data of these

<sup>1</sup> Civil Engineering Dept., Kyushu Electric Power Co., Inc., Fukuoka, Japan Fax: +81-92-761-4237

<sup>2</sup> Civil Engineering Dept., Kyushu Electric Power Co., Inc., Fukuoka, Japan Fax: +81-92-761-4237

<sup>3</sup> Civil Engineering Dept., Kyushu Electric Power Co., Inc., Fukuoka, Japan Fax: +81-92-761-4237

<sup>4</sup> Civil Engineering Dept., Kyushu Electric Power Co., Inc., Fukuoka, Japan Fax: +81-92-761-4237

<sup>5</sup> Nuclear Facilities Planning & Design Group, Taisei Corporation, Yokohama, Japan Fax: +81-45-224-2345

<sup>6</sup> Nuclear Facilities Planning & Design Group, Taisei Corporation, Yokohama, Japan Fax: +81-45-224-2345

<sup>7</sup> Nuclear Facilities Planning & Design Group, Taisei Corporation, Yokohama, Japan Fax: +81-45-224-2345

<sup>8</sup> Nuclear Facilities Planning & Design Group, Taisei Corporation, Yokohama, Japan Fax: +81-45-224-2345

earthquakes are shown in Figure 3 and Table 1. More information about strong-motion records during these sequences is shown in Kinoshita et al., 1999.

Because these sequences occurred near Sendai site as related above, and because they provided strong-motions in hard rock whose shear velocity is 1500m/s, the wave of these sequences was liable to have incident angles when they reached the site. This is why we used strong-motion records at Sendai site during the 1997 Kagoshima-ken hokuseibu earthquakes for our investigations.

In addition to this reason, there are the following two advantages of using these records. First, the peak accelerations of these records were the highest ever recorded at Sendai NPS, so that noise is relatively small compared with the other records. Second, as related in next chapter, wave incident angle is computed from observed records utilizing time lag between time histories at two sensors in rock. Therefore, time histories with minute pitches are required to evaluate accurate time lag between them. These records were digitized to discrete data with  $1/256 (= 0.00390625)$  second time pitches, and satisfy this request.

### ESTIMATION OF INCIDENT ANGLE OF OBSERVED EARTHQUAKE MOTIONS

Using observed several earthquake motions located in vertical array, the wave incident angle can be calculated with our developed method. On the other hand, the wave incident angle is given by the ray theory, using the relation between location of the hypocenter and the observation point. The incident angles obtained by two methods have been estimated as the similar values.

#### Incident Angle Obtained by Proposed Method

We derive the equation of incident angle for two stratums as shown in Figure 4. Each variable is defined in the figure. The soil properties used in the calculation are shear wave velocities,  $V_1, V_2, V_3$ , and thickness of layer,  $d_1, d_2$ . Here, propagation time,  $\Delta t$ , from point A to point B is needed for calculation of the incident angle at bottom layer,  $\theta_3$ . Considering the geometrical relation as illustrated in Figure 4,  $\overline{EB}$ ,  $\overline{CE}$ ,  $\overline{CA}$  and  $\overline{AD}$  are given by Equations (1), (2) and (3).

$$\overline{EB} = d_1 / \cos \theta_1, \quad \overline{CE} = d_2 / \cos \theta_2 \quad (1)$$

$$\overline{CA} = h_1 + h_2 = d_1 \tan \theta_1 + d_2 \tan \theta_2 \quad (2)$$

$$\overline{AD} = \overline{CA} \sin \theta_3 \quad (3)$$

Suppose that the incident wave is a plane wave, the time lag,  $\Delta t$ , from A to B is defined by the difference of the propagate time between  $\overline{CB}$  and  $\overline{AD}$ . The  $\Delta t$  are given by Equation (4)

$$\frac{d_1}{\cos \theta_1 V_1} + \frac{d_2}{\cos \theta_2 V_2} - \frac{\overline{CA} \sin \theta_3}{V_3} = f \Delta t \quad (4)$$

Here, using the Snell's law, that is,

$$\frac{\sin \theta_3}{V_3} = \frac{\sin \theta_2}{V_2} = \frac{\sin \theta_1}{V_1} = \text{const.}, \quad (5)$$

$\overline{\cos \theta_1}$  and  $\overline{\tan \theta_1}$  are deduced as a function of the incident angle at bottom layer,  $\theta_3$ .

$$\cos \theta_1 = \sqrt{1 - \sin^2 \theta_1} = \sqrt{1 - \sin^2 \theta_3 \left( \frac{V_1}{V_3} \right)^2} \quad (6)$$

$$\tan \theta_1 = \frac{\sin \theta_1}{\cos \theta_1} = \sin \theta_3 \frac{V_1}{V_3} \frac{1}{\sqrt{1 - \sin^2 \theta_3 \left( \frac{V_1}{V_3} \right)^2}} \quad (7)$$

By the same mathematical operation,  $\cos \theta_2$  and  $\tan \theta_2$  are deduced as a function of  $\theta_3$ . Then, substituting Equations (2), (6) and (7) into Equation (4), and extending to  $N-1$  stratum, we have the following equation.

$$\sum_{i=1}^{N-1} \frac{d_i \sqrt{V_N^2 - V_i^2 \cos^2 \theta_N}}{V_N \cdot V_i} = \Delta t \quad (8)$$

Solving the above equation, we have the wave incident angle at bottom,  $\theta_N$ . Apparently, incident angle of each layer boundary can be obtained by substituting  $\theta_N$  into Equation (5). Especially, the direction of wave propagation is assumed to be vertical, that is,  $\theta_N = 0$ , Equation (8) is transformed to

$$\sum_{i=1}^{N-1} \frac{d_i}{V_i} = \Delta t. \quad (9)$$

The time lag,  $\Delta t$ , calculated by Equation (9) means the maximum propagation time, so that Equation (8) is effective when observed  $\Delta t$  is smaller than that obtained by Equation (9). The  $\Delta t$  can be given from the observed records in some way. In this paper, we propose that  $\Delta t$  is evaluated from using a cross-correlation function between A and B point.

Finally, using the 24 observed earthquake motions, which are described in section 2,  $\Delta t$  and wave incident angle near ground surface in Sendai site are practically evaluated. Figure 5 shows that examples of cross-correlation function between GL-70m and GL-130m (sensor locations are shown in Figure 2). The  $\Delta t$  is taken the time at which the cross-correlation function have a maximum value. Equation (8) provides wave incident angle near ground surface of each earthquake as shown in Table 2. Evaluated wave propagation time,  $\Delta t$ , is evaluated at 1/256 (s), since observed records are digitized to discrete data with 1/256 (s). Incident angle on X-Z plane can not be calculated from observed record of July 26, 1997, because its  $\Delta t$  is beyond the maximum propagation time obtained by Equation (9), that is, 60 (m)/1500 (m/s)=0.04 (s), where, 60 (m) is distance between GL-70m and GL-130m. Calculated incident angles are varied for different earthquakes. The mean incident angle on both X-Z and Y-Z plane is about 38°.

### Incident Angle Obtained by the Ray Theory

The underground structure of the earth's crust around Sendai site has been clarified in the literature [Ono et al., 1978]. As shown in Table 3, an underground model for ray tracing analysis based on the ray theory is constructed with layers overlying half-space, including surface soil with S-wave velocity of 1.5km/sec on which Sendai NPS structure is built. According to the literature [Kikuchi and Yamanaka, 1997], it is estimated that mainshock on March 26 have fault plane of 15km length and 7.5km depth, and fault of May 13 mainshock consists of two fault planes of 5.0km depth. These faults are erected vertically, that is, not inclined. Figure 6 illustrates the relation between Sendai site and these faults.

Using above analysis model, the ray tracing analysis is carried out for earthquakes on March 26 and May 13 in order to investigate the S-wave incident angle near ground surface. The representative ray paths, their travel time and wave incident angles near ground surface for S-wave are shown in Figure 7. As shown in this figure, these ray paths take similar travel time. This means that all ray paths illustrated in Figure 7 may contribute to principal part of S-wave at ground surface. Each ray path provides a wave incident angle, respectively. Figure 7 shows that the wave incident angle varies from about 25° to 37° according to ray paths but not significantly differ with earthquakes.

## THE EFFECT OF WAVE INCIDENT ANGLES ON STRUCTURAL RESPONSES

As described above, we could recognize obliquely incident waves on the present ground. In this section, the effect of wave incident angle on structural responses is examined by using two-dimensional finite element (2DFE) method. Where, the effect of wave incident angle is evaluated as the transfer function, which is the ratio of acceleration on basemat of R/B to the free field motion.

Figure 8 shows 2DFE model for ground of Sendai site, which is homogeneous and isotropic having the shear wave velocity of 1.5 km/s. The critical damping ratio, density and Poisson's ratio of ground were assumed 2%, 2700 kg/m<sup>3</sup> and 0.373, respectively. The analysis model was used the energy transmitting boundary at the both sides of model as shown in Figure 8. The boundary condition at the bottom of ground was settled damping boundary of horizontal and vertical directions respectively. While SV-wave is dealt with for horizontal direction, P-wave for vertical direction.

Figure 9 shows calculated transfer functions for different wave incident angle. The transfer function is defined as the acceleration on top of R/B base mat normalized to the surface free-field response. As shown in Figure 9(a), the transfer functions of horizontal direction fluctuate significantly in the domain of higher frequency than 4.0 s<sup>-1</sup>. The transfer functions with wave incident angle of 0° to 30° are same to each other. The transfer functions with wave incident angle of greater than 40° shows a similar tendency to those of 0° to 30°. On the contrary, Figure 9(b) shows that vertical transfer functions are same to each other up to 50°. The amplitude of transfer function is 1.0 up to about 10 s<sup>-1</sup>, and goes down around 13 s<sup>-1</sup> and 16 s<sup>-1</sup> subject to existence of structure.

## CONCLUSIONS

These results lead to the conclusions as follows.

- (a) We proposed the calculation method of wave incident angle of actual earthquake motion. The developed method in this study indicated obliquely incident waves near ground surface of rock site. The incident angles, which are calculated from actual earthquakes by proposed method, correspond to those by the ray theory.
- (b) The effect of the wave incident angle on structural responses, which is evaluated as the transfer function of basemat of R/B to the free field, was examined. For Sendai site, the wave incident angle of up to 30° had the same effect on structural responses as vertical incident had. Even an incident angle of greater than 40° did not affect them very much. In other words, it can be considered that obliquely incident waves do not necessarily cause bat effects to the structure.

## REFERENCES

- Kikuchi, M. and Yamanaka, Y. (1997), "Rapture process of the northern Kagoshima prefecture, Japan, earthquake of March 26, 1997", *Programme and Abstracts of Seismological Society of Japan, No.2, P81* (in Japanese)
- Kiyohara, K., Sono, Y., Kinoshita, D. Masao, T. and Ugata, T. (1999), "Earthquake observation and simulation analyses of Sendai nuclear power station on the 1997 Kagoshima-ken hokuseibu earthquakes", *Proceedings 15th Structural Mechanics in Reactor Technology, K*
- Ono, K., Ito, K., Hasegawa, I., Ichikawa, K., Iizuka, S., Kakuta, T. and Suzuki, H. (1978), "Explosion seismic studies in south Kyusyu especially around the Sakurajima volcano", *J.Phys.Earth, 26, Suppl.*, S309-S319

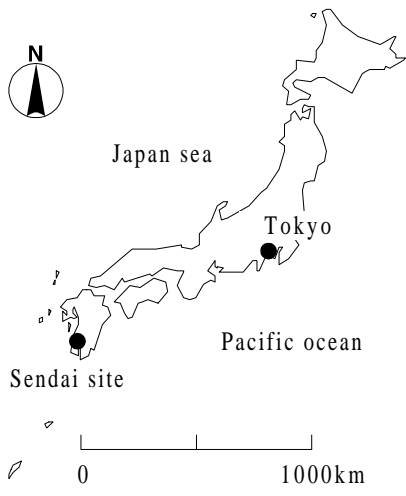
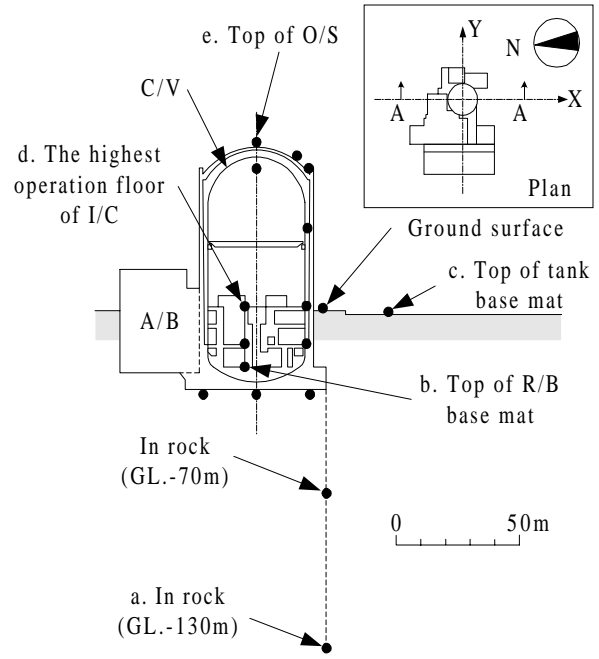


Figure 1: Map of Sendai nuclear power station site



A-A section  
Figure 2: Sensor locations

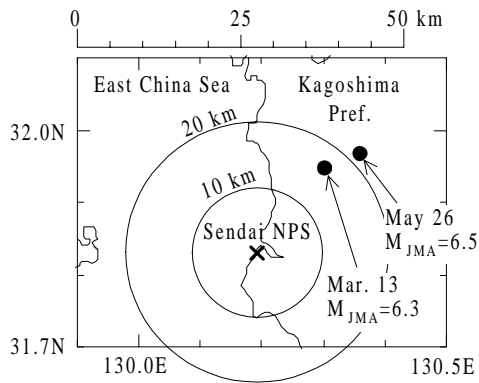


Figure 3: Epicenter of mainshocks

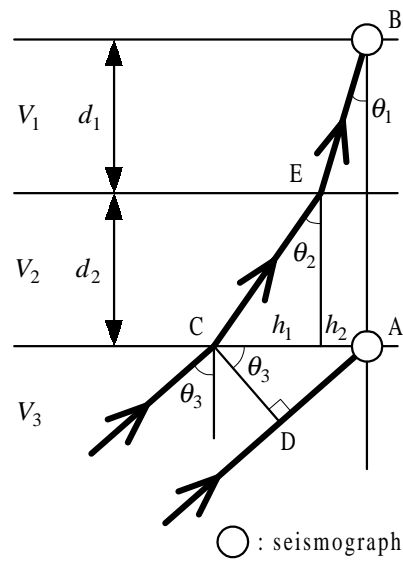
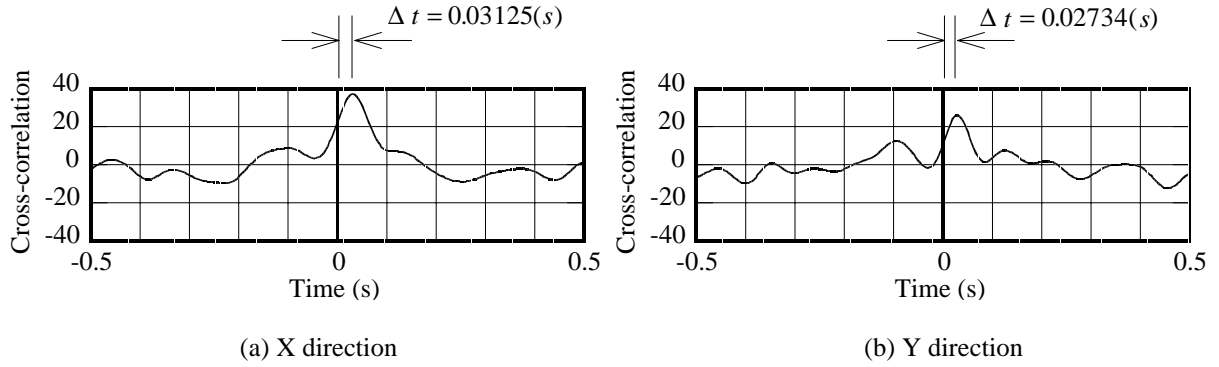


Figure 4: Plane wave transmits in the layered media

**Table 1: Data of mainshocks**

Date* (Japanese time)	Mar. 26,1997 17:31	May 13,1997 14:38
Latitude*	31° 58.1'N	31° 56.6'N
Longitude*	130° 21.6'E	130° 18.3'E
JMA Magnitude*	6.5	6.3
Depth*	11.8km	9.2km
Epical distance	22.0km	16.5km
Hypocentral distance	25.0km	18.9km

\* : Issued by Japanese Meteorological Agency (JMA)



**Figure 5: Examples of cross-correlation function between GL.-130m and GL.-70m (March 26, mainshock)**

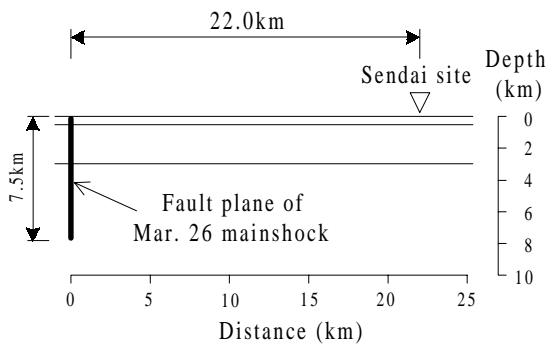
**Table 2: Propagation times and incident angles**

Date	Time (Japanese Time)	Propagation time from GL.-130m to GL.-70m ( $\Delta t$ (s) )		Estimated incident angle ( $^{\circ}$ )	
		X	Y	X-Z plane	Y-Z plane
3/26/1997*1	17:31	0.03125	0.02734	38.6	46.9
3/26/1997	18:05	0.02734	0.02734	46.9	46.9
3/26/1997	22:24	0.02734	0.02734	46.9	46.9
3/26/1997	22:48	0.02734	0.03125	46.9	38.6
3/31/1997	9:04	0.02344	0.02734	54.1	46.9
4/3/1997	4:33	0.03516	0.03516	28.5	28.5
4/3/1997	5:13	0.03516	0.03125	28.5	38.6
4/4/1997	2:33	0.03516	0.03125	28.5	38.6
4/5/1997	13:24	0.02734	0.03125	46.9	38.6
4/9/1997	23:20	0.03125	0.03125	38.6	38.6
4/9/1997	23:23	0.02734	0.02344	46.9	54.1
4/15/1997	9:33	0.03516	0.03125	28.5	38.6
5/3/1997	9:00	0.03125	0.03516	38.6	28.5
5/13/1997*1	14:38	0.02734	0.03125	46.9	38.6
5/14/1997	8:32	0.03125	0.02734	38.6	46.9
5/25/1997	6:11	0.00391	0.02734	84.4	46.9
6/27/1997	14:12	0.03125	0.03125	38.6	38.6
7/26/1997	18:36	0.05078	0.03125	*2	38.6
11/11/1997	21:41	0.03125	0.03125	38.6	38.6
12/14/1997	0:19	0.03516	0.03906	28.5	12.4
12/25/1997	0:17	0.03906	0.03516	12.4	28.5
12/25/1997	18:58	0.03516	0.03516	28.5	28.5
1/10/1998	14:01	0.03516	0.03516	28.5	28.5
1/10/1998	14:02	0.03906	0.03125	12.4	38.6
Mean				38.1	38.1

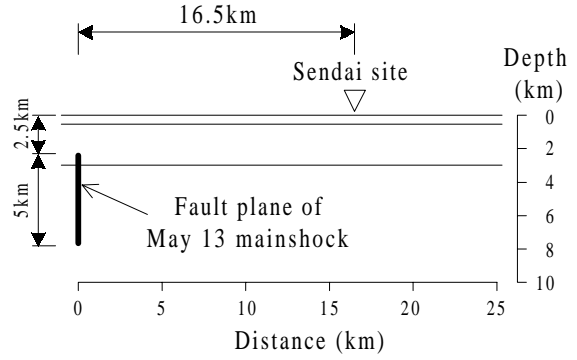
\*1:Mainshock \*2:Not calculated by Equation (8) because observed  $\Delta t$  is beyond maximum propagation time

**Table 3: Underground model for ray tracing analysis**

Depth (km)	Thickness (km)	S-wave velocity (km/s)
0.54	0.54	1.5
3.0	2.46	2.5
22.0	19.0	3.4

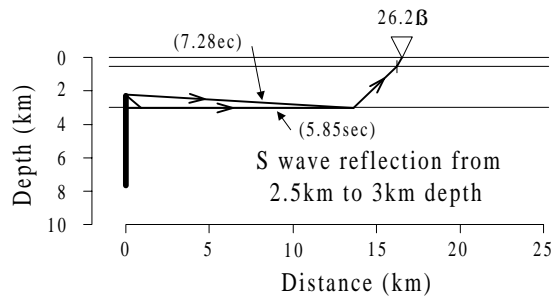
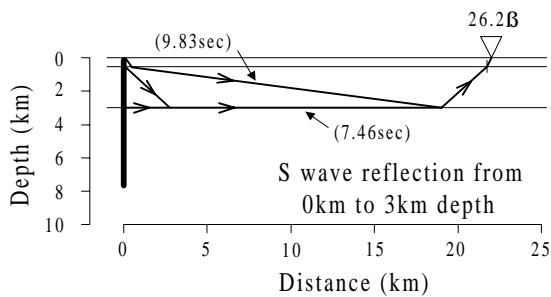
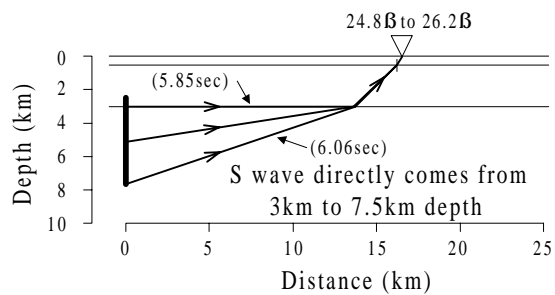
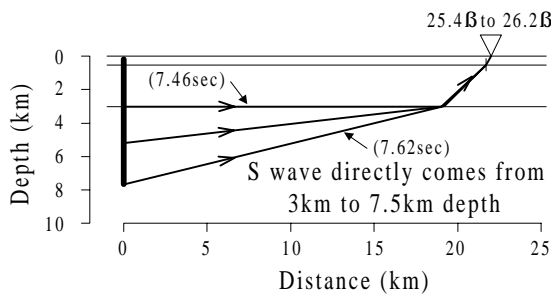
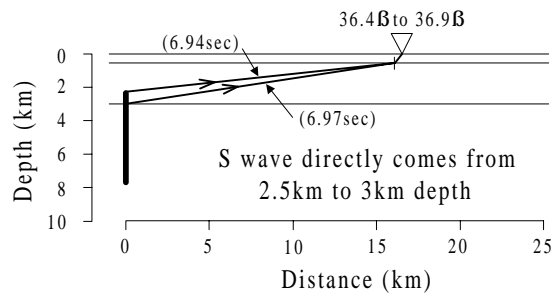
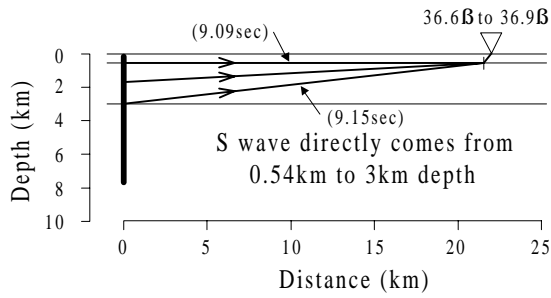


**(a) March 26, 1997**



**(b) May 13, 1997**

**Figure 6: Locations of Sendai site and fault planes for ray tracing analysis**



**(a) March 26, 1997**

**(b) May 13, 1997**

**Figure 7: Representative ray paths, their travel time and incidence angles near surface**

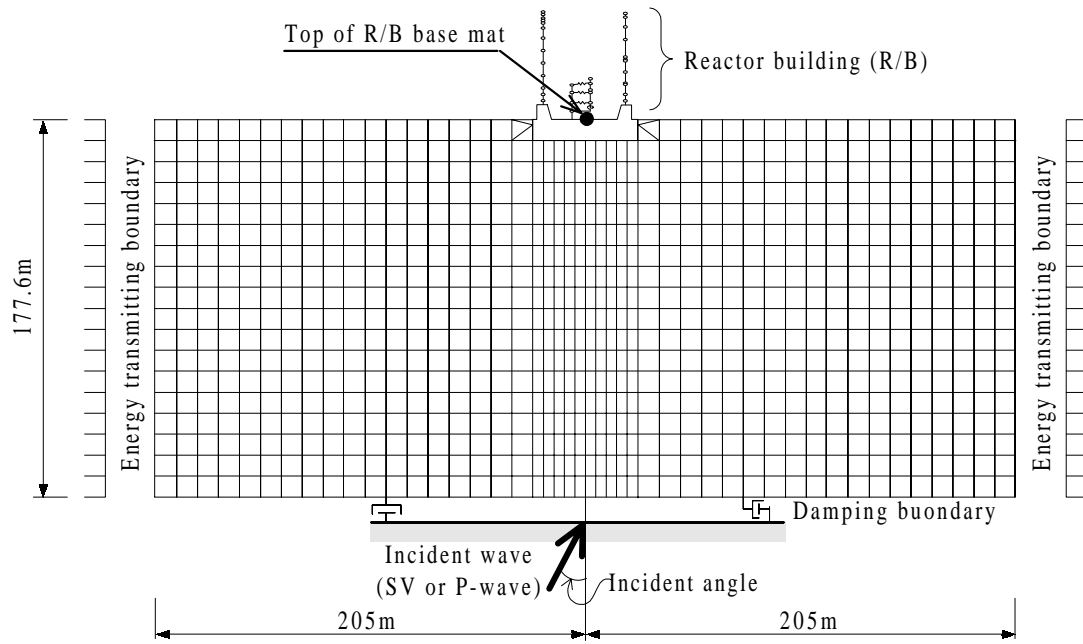


**Figure 8: Analysis model for 2D finite element**

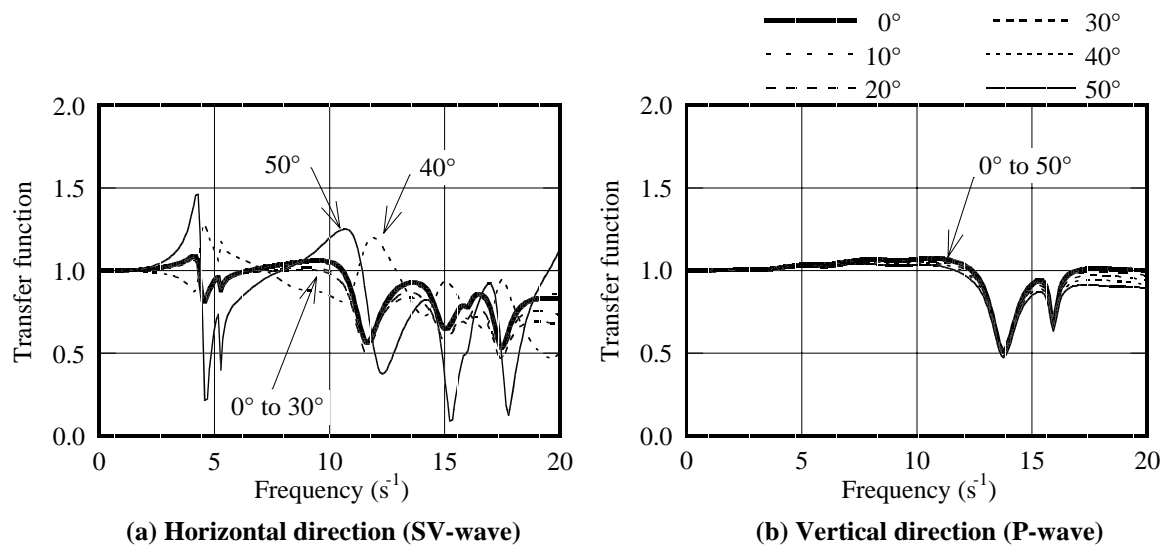


**Figure 9: Transfer function for different wave incident angles**